Direct Observation of an Inhomogeneous Chlorine Distribution in $CH_3NH_3PbI_{3-x}Cl_x$ Layers: Surface Depletion and Interface Enrichment

David E. Starr,[a,*] Golnaz Sadoughi,[b] Evelyn Handick,[a] Regan G. Wilks,[a,c] Jan-Hendrik Alsmeier,[a] Leonard Köhler,[a] Mihaela Gorgoi,[d] Henry Snaith,[b,*] and Marcus Bär[a,c,d]

[a]*Renewable Energies, Helmholtz-Zentrum Berlin für Materialien und Energie GmbH, D-14109 Berlin, Germany*

[b]*Department of Physics, Clarendon Laboratory, University of Oxford, Oxford, OX1 3PU, UK*

[c]*Energy Materials In-situ Laboratory Berlin (EMIL), Helmholtz-Zentrum Berlin für Materialien und Energie GmbH, D-12489 Berlin, Germany*

[d]*Institute for Methods and Instrumentation for Synchrotron Radiation Research, Helmholtz-Zentrum Berlin für Materialien und Energie GmbH, D-12489 Berlin, Germany*

[e]*Institut für Physik und Chemie, Brandenburgische Technische Universität Cottbus-Senftenberg, D-03046 Cottbus, Germany*

Supporting Information

HAXPES information depth estimation

The data points in Figure S. I. 1 are normalized Pb $4f_{7/2}$ and Ti $2p_{3/2}$ XPS peak areas extracted from spectra simulated with SESSA v1.3 as a function of perovskite layer thickness.[1] The atomic density used for the perovskite layer in the simulations was 4.996 x 10^{22} atoms/cm^3 which was calculated from the known bulk density (4.2864 g/cm^3) of $CH_3NH_3PbI_3$.[2] A band gap of 1.5 eV was used for the perovskite layer in the simulations.[3] For the TiO_2 layer an atomic density of 9.57 x 10^{22} atoms/cm^3 (based on the bulk density of rutile TiO_2, 4.26 g/cm^3) and a band gap of 3.10 eV was used.[4,5] Spectra were simulated at photon energies of 2003 eV and 6009 eV and the experimental geometry (X-ray incident angle of 3.7° and electron exit angle of 93.7°

from the sample surface plane, where 0° is defined as in the surface plane in the direction of the incoming X-ray beam) used in our study. The simulated Pb $4f_{7/2}$ and Ti $2p_{3/2}$ peak areas were normalized by the Pb $4f_{7/2}$ peak area simulated for a 1000 nm thick perovskite film (Pb $4f_{7/2}^{\infty}$) and the Ti $2p_{3/2}$ peak area simulated for a bulk TiO_2 with no perovskite film (Ti $2p_{3/2}^{0}$), respectively.

The solid lines in Figure S. I. 1 are fits to the simulated data assuming homogeneous, smooth, layer-by-layer growth of the perovskite on TiO_2. In this growth model the normalized substrate signal (Ti $2p_{3/2}$/ Ti $2p_{3/2}^{0}$) will decrease with overlayer thickness according to $\exp[-t/\lambda]$ and the normalized overlayer signal (Pb $4f_{7/2}$/ Pb $4f_{7/2}^{\infty}$) will increase according to $(1- \exp[-t/\lambda])$ where t is the thickness of the perovskite layer and λ is the characteristic escape depth of electrons of a specific kinetic energy in the overlayer material.[6] Pb $4f_{7/2}$ photoelectrons will have kinetic energies of approximately1860 eV and 5865 eV for incident photon energies of 2003 eV and 6009 eV, respectively. Ti $2p_{3/2}$ photoelectrons will have kinetic energies of ~1540 eV and 5545 eV for incident photon energies of 2003 eV and 6009 eV, respectively. The characteristic escape depths obtained from the fitted data are 2.74 nm for ~1540 eV photoelectrons, 3.34 nm for ~1860 eV photoelectrons, 8.35 nm for 5545 eV photoelectrons, and 8.98 nm for 5865 eV photoelectrons. Linear interpolation from these values provides characteristic escape depths for Cl 2p photoelectrons (kinetic energies of approximately 1800 eV and 5805 eV) of ~3.2 nm and 8.8 nm for spectra taken with photon energies of 2003 eV and 6009 eV, respectively. Approximating the maximum information depths as three escape depths leads to maximum information depth estimations of ~10 nm and 26 nm for Cl 2p photoelectrons in spectra taken with 2003 eV and 6009 eV photon energies, respectively.

HAXPES estimate of minimum detectable amount of Cl

Based on the spectra presented in Figures 1 and 2 we can estimate the minimum amount of Cl that would be detectable at photon energies of 2 keV and 6 keV. To do this we have added simulated Cl 2p peaks of varying areas with the same binding energy and peak shape as the fitted Cl 2p peak in Figure 1 to the spectra in Figure 2. The Cl 2p peak areas used were 0.01, 0.02, 0.03, 0.04, and 0.05 times the peak area of the I 4s peak area, and the resulting spectra are shown in Figure S. I. 2. From these spectra we conservatively estimate that we would be able to detect Cl 2p peaks with areas ~0.02 to 0.03 times the I 4s peak area for both, the 2 and 6 keV measurements. Below we use a value of 0.025 times the I 4s peak area for our estimate. Since the photon flux, electron energy analyzer transmission characteristics and the information depth will be very similar for the Cl 2p and I 4s peaks regardless of the incident photon energy used, to convert the estimated minimum detectable relative intensity of the Cl 2p peak to a maximum relative amount of Cl (for a specific photon energy), we need only to consider the relative photoionization cross-sections for the Cl 2p and I 4s core levels at 2 keV and 6 keV. When calculating the cross-sections we have included dipole and higher order terms and, when necessary, used linear interpolation between published values of the higher order terms to derive the cross-sections for the photoelectron kinetic energies used in our experiment. Based on the values provided by Trzhaskovskaya[7,8] and our HAXPES experimental geometry ($\theta \approx 0°$, $\varphi \approx 90°$) the cross-section ratio $\sigma_{Cl\ 2p} : \sigma_{I\ 4s}$ is approximately 1.034 for the spectra taken with 2 keV photons and 0.163 for the spectra taken with 6 keV photons. This leads to maximum relative amounts of Cl to I (assuming similar distributions of Cl and I within the measurement volume) of 0.025/1.034 = 0.024 and 0.025/0.163 = 0.15 for the 2 keV and 6 keV photon energy spectra, respectively. Since the chemical formula for the perovskite is $CH_3NH_3PbI_{(3-x)}Cl_x$ and x/(3-x) is the relative amount of Cl to I, we can estimate maximum values of x for the spectra taken at the two photon energies. We find that for spectra taken with 2 keV $x < 0.07$ and for the spectra taken

with 6 keV $x < 0.40$. We note that the spectra taken with 6 keV have approximately 2.5 times the information depth of the spectra taken with 2 keV (see above information depth estimation).

Depletion of Cl in the surface region

Figure S.I. 3 shows the Cl 2p region as a function of temperature. The photon energy used was 2 keV and the information depth is estimated to be approximately 10 nm. By approximately 50 °C the Cl 2p signal has decreased to our detection limit indicating that the relative amount of Cl to I has fallen below approximately 0.024 that of I (see above).

FY-XAS information depth estimation

The attenuation length of photons in the perovskite depends on the photon energy and the concentration of Cl, which is unknown but small throughout most of the material (see above). To estimate the X-ray attenuation length we have calculated X-ray attenuation lengths for perovskite films with two different Cl concentrations: one with a lower Cl concentration than what we observe experimentally (a $CH_3NH_3PbI_3$ layer, i.e., a perovskite layer without any Cl) and another with a higher Cl concentration than what we observe experimentally (a $CH_3NH_3PbI_2Cl$ layer, i.e., a perovskite layer with a Cl : I ratio of 0.5).[9] (A density of 4.286 g/cm^3 for the perovskite film[10] and an incidence angle of 90° from the sample surface were used for the calculations.) Just below the Cl K edge (2818 eV) the attenuation lengths are approximately 1.75 and 1.70 μm for the Cl-free and $CH_3NH_3PbI_2Cl$ layers, respectively. At the Cl K edge (2821 eV) the attenuation lengths are 1.76 and 1.59 μm and at 2845 eV they are 1.79 and 1.62 μm for the Cl-free and $CH_3NH_3PbI_2Cl$ layers, respectively. Since the Cl concentration in the perovskite layer is small – but possibly non-zero – we estimate that the attenuation length is approximately 1.65 μm. However, due to the grazing incidence of the photons the information depth of the FY-XAS

measurements is determined by how deeply the incident photons penetrate beneath the sample surface. This value is equal to the attenuation length multiplied by a factor of cos(86.3°), or approximately 100 nm.

Cl K edge FY-XAS minimum detectable amount estimation

The Cl K edge absorption signal for the perovskite layer shown in Figure 3 may arise from Cl distributed throughout the perovskite layer with a concentration below the HAXPES detection limit, Cl with a concentration above the HAXPES detection limit but located deeper than the information depth of the HAXPES measurements (e.g., near or at the perovskite / TiO_2 interface), or a combination of these explanations. Estimating the Cl detection limit for the Cl K edge FY-XAS measurements is useful to determine which of these cases is possible. To do this we have used the following procedure: First, X-ray fluorescence (XRF) spectra of the Pb M_α and Cl K_α region were collected with incident photon energies below (2810 eV) and above (2845 eV) the Cl K_β absorption edge for $PbCl_2$. Second, we recast the spectrum taken at 2810 eV into an XRF spectrum representative of one used to collect the Cl K edge FY-XAS signal shown in Figure 3 by appropriately scaling the Pb M_α signal intensity. Third, we use the XRF spectrum taken with a photon energy of 2845 eV to calculate a Cl-to-Pb sensitivity factor. Lastly, we add Cl K_α signals for various values of x (the Cl-to-Pb atomic ratio in $CH_3NH_3PbI_{3-x}Cl_x$) to the appropriately scaled spectrum taken at 2810 eV using the calculated Cl-to-Pb sensitivity factor and estimate at what value of x we would have a large enough signal to see it in the Cl K edge FY-XAS spectrum.

The XRF spectrum shown in Figure S. I. 4 is the sum of the signal collected for 120 s. The XRF signal used for the FY-XAS spectrum of the perovksite layer in Figure 3 was collected with a 1 s dwell time at each incident photon energy. Therefore, the signal to noise ratio of the

XRF spectra in Figure S.I. 4 far exceeds the signal to noise ratio of the XRF signal used for the FY-XAS spectrum, and this needs to be taken into account to accurately estimate a detection limit. When noise is random and uncorrelated the variance is additive implying that the variance of the XRF spectrum in Figure S. I. 4 is 120 times the variance of the XRF signal used for the FY-XAS spectrum (i.e. $\sigma_1^2 = 120 \times \sigma_2^2$, where σ_1 and σ_2 are the standard deviations of the XRF measurements for the data in Figure S. I. 4 and the Cl K edge FY-XAS spectra respectively, and σ_1^2 and σ_2^2 are the variances). To take this into account we have fitted the XRF spectrum taken with 2810 eV (c.f. Figure S. I. 5, red curve) and subtracted the fit from the data resulting in the residuals shown by the blue dots in Figure S. I. 5. The standard deviation, σ_1, of the residuals is 225.09 giving a variance of $\sigma_1^2 = 50665.5$ leading to $\sigma_2 = 20.54$. We will now scale the fitted spectrum by scaling the Pb M_α signal intensity to a level representative of one used to collect the Cl K edge FY-XAS signal shown in Figure 3 and add to this Gaussian noise with a standard deviation of 20.54.

To produce an XRF spectrum representative of the XRF signal used for the FY-XAS spectrum we have first divided the fit of the XRF spectrum taken with 2810 eV (red curve of Figure S.I. 5) by 120 (this converts the curve from counts into counts per second). Next, we need to account for differences in molar densities of Pb in the perovskite compared to $PbCl_2$, (since XRF is sensitive to molar concentration), differences in photon flux between the XRF and FY-XAS measurements, differences in photon attenuation lengths between $PbCl_2$ and the perovskite, and differences in experimental geometry between the two measurements. That is, we estimate the intensity of the Pb M_α XRF signal used for the FY-XAS measurements of the perovskite, $I_{Pb\,M}^{perov.} \propto$, by,

$$I_{Pb\,M_\propto}^{perov.} = I_{Pb\,M_\propto}^{PbCl_2}\left(\frac{\lambda_{Pb\,M_\propto}^{perov.}}{\lambda_{Pb\,M_\propto}^{PbCl_2}}\right)\left(\frac{cos\theta_{Pb\,M_\propto}^{perov.}}{cos\theta_{Pb\,M_\propto}^{PbCl_2}}\right)\left(\frac{f_{Pb\,M_\propto}^{perov.}}{f_{Pb\,M_\propto}^{PbCl_2}}\right)\left(\frac{N_{Pb}^{perov.}}{N_{Pb}^{PbCl_2}}\right)$$

where $I_{Pb\,M_\propto}^{PbCl_2}$ is the Pb M_α XRF signal from $PbCl_2$ in counts per second, $\lambda_{Pb\,M_\propto}^{perov.}$ and $\lambda_{Pb\,M_\propto}^{PbCl_2}$ are the photon attenuation lengths through the perovskite and $PbCl_2$ respectively, $\theta_{Pb\,M_\propto}^{perov.}$ and $\theta_{Pb\,M_\propto}^{PbCl_2}$ are the angles between the incident photons and the surface normal for the FY-XAS measurements of the perovskite and the XRF measurements of $PbCl_2$ respectively, $f_{Pb\,M_\propto}^{perov.}$ and $f_{Pb\,M_\propto}^{PbCl_2}$ are the incident photon fluxes for the FY-XAS measurements of the perovskite and XRF measurements of $PbCl_2$ respectively, and $N_{Pb}^{perov.}$ and $N_{Pb}^{PbCl_2}$ are the molar densities of Pb in the perovskite and $PbCl_2$ respectively.

The density of $PbCl_2$ is 5.85 g/cm^3 and its molecular weight is 278.10 g/mol, the molar concentration is therefore 0.021 mol/cm^3. Similarly the molar concentration of $CH_3NH_3PbI_3$ can be found to be 0.00691 mol/cm^3. This means that $\left(\frac{N_{Pb}^{perov.}}{N_{Pb}^{PbCl_2}}\right)$ is 0.00691/0.021 = 0.329. For $\left(\frac{\lambda_{Pb\,M_\propto}^{perov.}}{\lambda_{Pb\,M_\propto}^{PbCl_2}}\right)$ we have used the value estimated above for the perovskite ($\lambda_{Pb\,M_\propto}^{perov.}$ = 1.65 μm) and $\lambda_{Pb\,M_\propto}^{PbCl_2}$ = 0.780 μm [9] leading to $\left(\frac{\lambda_{Pb\,M_\propto}^{perov.}}{\lambda_{Pb\,M_\propto}^{PbCl_2}}\right)$ = 2.11. The XRF spectrum shown in Figure S. I. 4, left, and S. I. 5 were taken with θ = 40° while the data shown in Figure 3 was taken with θ = 86.3°

leading to $\left(\frac{cos\theta_{Pb\,M_{\propto}}^{perov.}}{cos\theta_{Pb\,M_{\propto}}^{PbCl_2}}\right)$ = 0.08. Last a small correction to the relative flux estimated from the relative measurements of I_0 for the two measurements, $\left(\frac{f_{Pb\,M_{\propto}}^{perov.}}{f_{Pb\,M_{\propto}}^{PbCl_2}}\right)$ = 1.29, was applied. The fitted spectrum in Figure S. I. 5 (red line) has been scaled by these factors and to this scaled spectrum Gaussian noise with a standard deviation of σ_2 = 20.54 has been added. The resulting spectrum is shown in Figure S. I. 6, black dots. This spectrum approximates the XRF spectrum that is used to collect the Cl K edge FY-XAS spectrum shown in Figure 3.

We add to this spectrum Cl K_α peaks with the same shape as in Figure S. I. 4, right, with an intensity of $I_{Pb\,M_{\propto}}^{perov.}$ multiplied by a Cl-to-Pb sensitivity factor and increasing values of x (the Cl to Pb ratio in the perovskite) to estimate $I_{Cl\,K_{\propto}}^{perov.}$ for increasing values of x in the perovskite. The Cl-to-Pb sensitivity factor is estimated by integrating the area under the Pb M_α and Cl K_α peaks in the spectrum taken with 2845 eV photon energy (Figure S. I. 4, right) and using the known Cl : Pb concentration ratio in $PbCl_2$ (2 : 1). The resulting Cl-to-Pb sensitivity factor is 0.397. In Figure S. I. 6, simulated spectra for x = 0.0 (black dots), x = 0.05 (red dots), x = 0.10 (blue dots), x = 0.20 (green dots), x = 0.30 (orange dots), x = 0.40 (purple dots) and x = 0.50 (pink dots) are shown. We have also included the appropriately scaled fitted spectrum of Figure S. I. 5 as red lines with each of these spectra to act as a visual aid. The energy window monitored for the FY-XAS spectra is indicated by the light blue box in Figure S. I. 6. Figure S. I. 6 shows that Cl concentrations below ~ x = 0.3 to 0.4 could not be detected in our FY-XAS measurements. This is similar to the detection limit for the HAXPES measurements taken at 6

keV for depths to 26 nm. Since the FY-XAS spectra average over the entire thickness of the perovskite film and the surface of the perovskite is depleted of Cl to $x < 0.07$ to a depth of ~ 10 nm, this indicates that the concentration of Cl must be higher than $x = 0.40$ at depths of > 26 nm beneath the surface of the perovskite film, i.e. close to the TiO_2 interface.

Figure S.I. 1

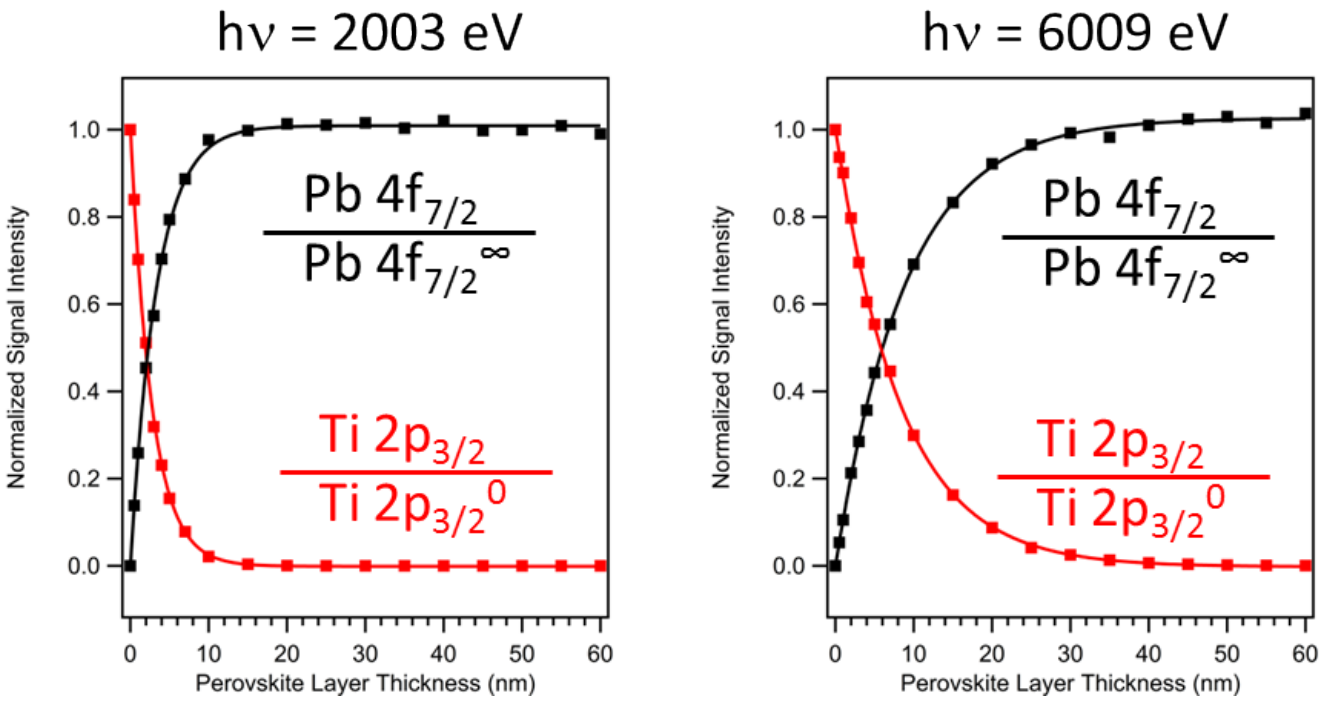

Figure S. I. 1: Simulated, normalized Pb $4f_{7/2}$ (black) and Ti $2p_{3/2}$ (red) signal intensity as a function of perovskite layer thickness at photon energies of 2003 eV and 6009 eV. The points are calculated from the simulation and the lines are fits to the data points assuming layer by layer growth of the perovskite film on the TiO2 substrate. See text for simulation details.

Figure S. I. 2

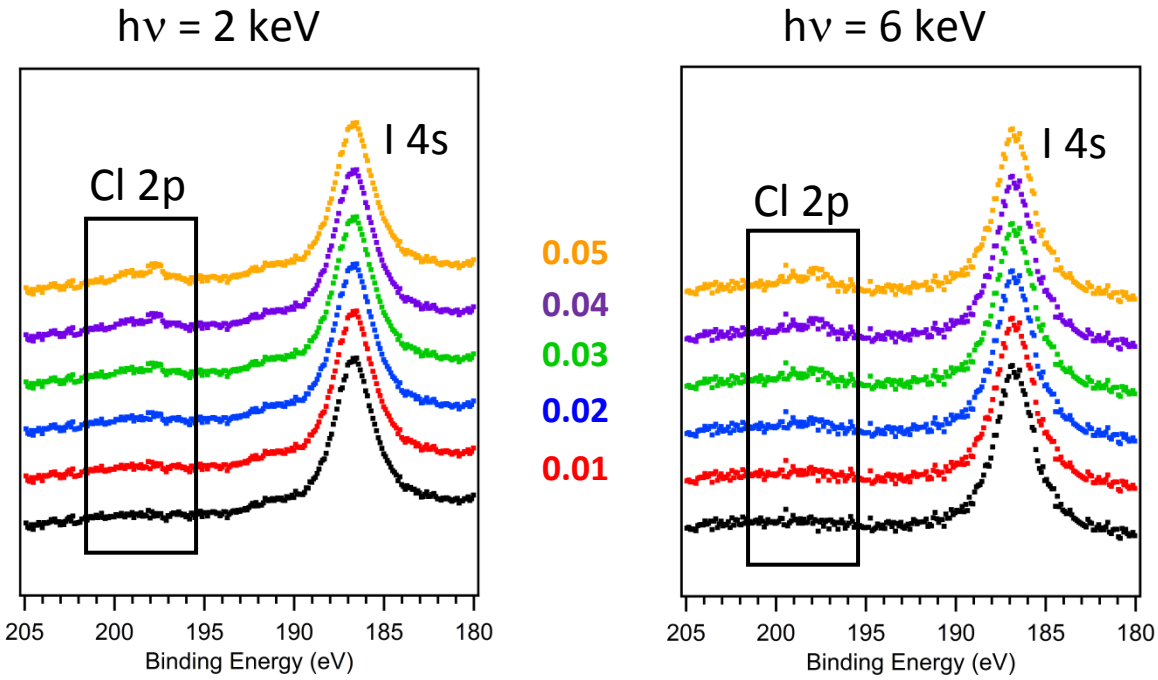

Figure S. I. 2: The Cl 2p and I 4s spectra from Figure 2 (black) at two photon energies 2 keV and 6 keV. To the other spectra a Cl 2p peak with the same peak parameters as the fitted spectrum in Figure 1 has been added. The area of this additional Cl 2p peak is 0.01 (red), 0.02 (blue), 0.03 (green), 0.04 (purple), or 0.05 (orange) times the area of the I 4s peak.

Figure S. I. 3

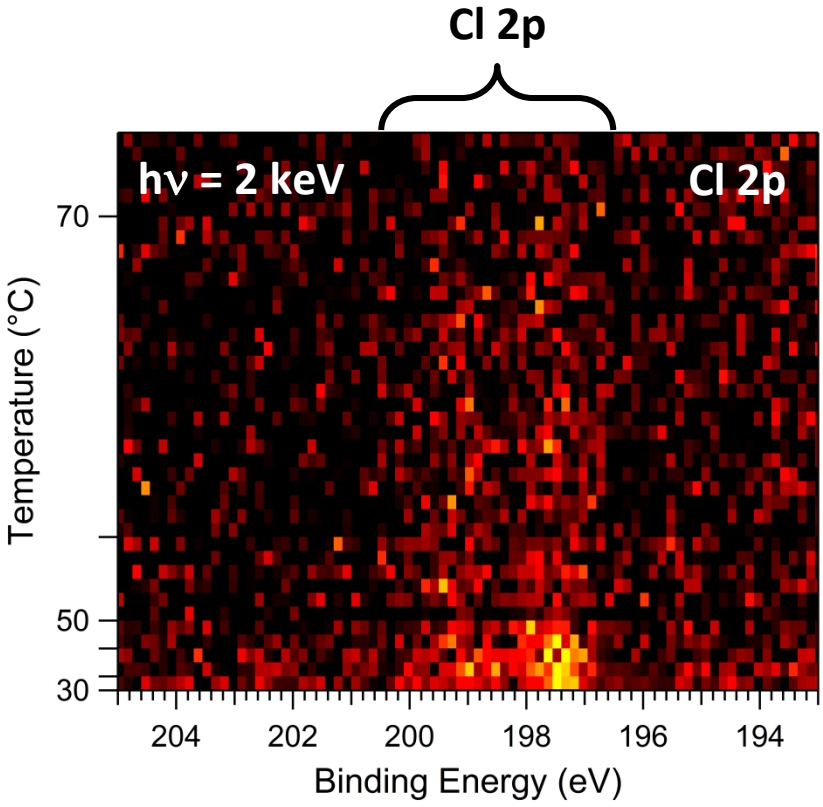

Figure S. I. 3: The Cl 2p region as a function of temperature taken with a photon energy of 2 keV. Yellow indicates higher intensities in the plot. The Cl 2p region is indicated at the top of the plot.

Figure S. I. 4

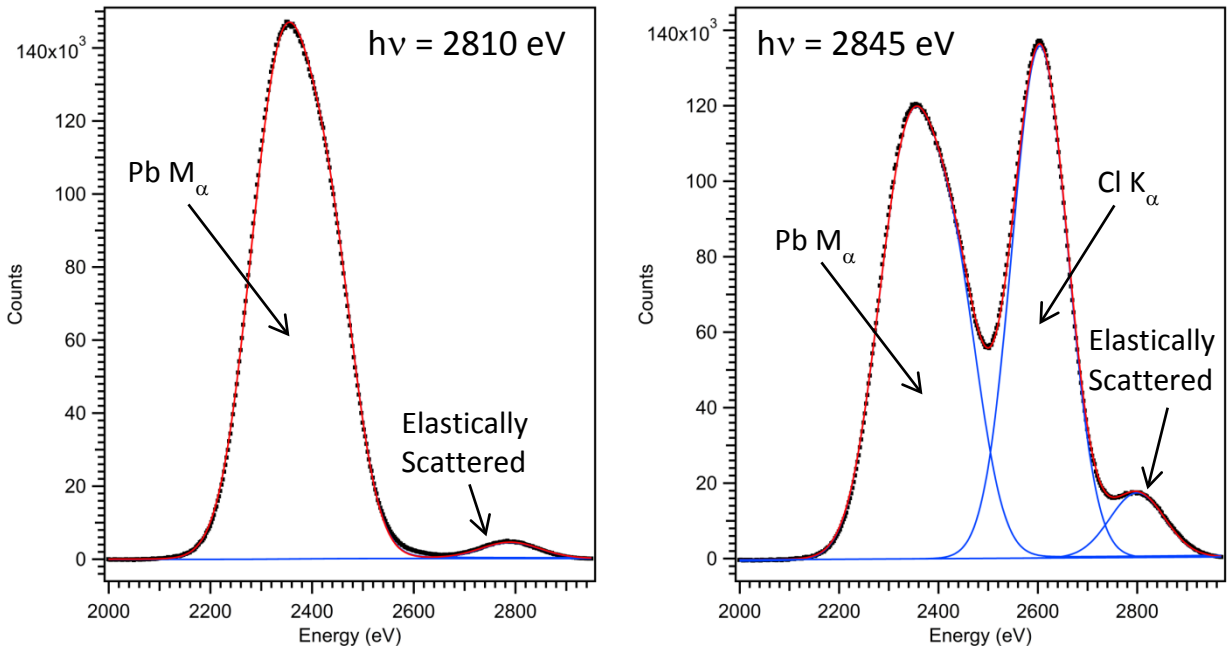

Figure S. I. 4: XRF spectra of $PbCl_2$ taken with photon energies of 2810 eV (left) and 2845 eV (right), black dots. The spectra have been fitted with peaks for Pb M_α and Cl K_α emission, blue curves. The red curve is the sum of the curves as a result of fitting.

Figure S. I. 5

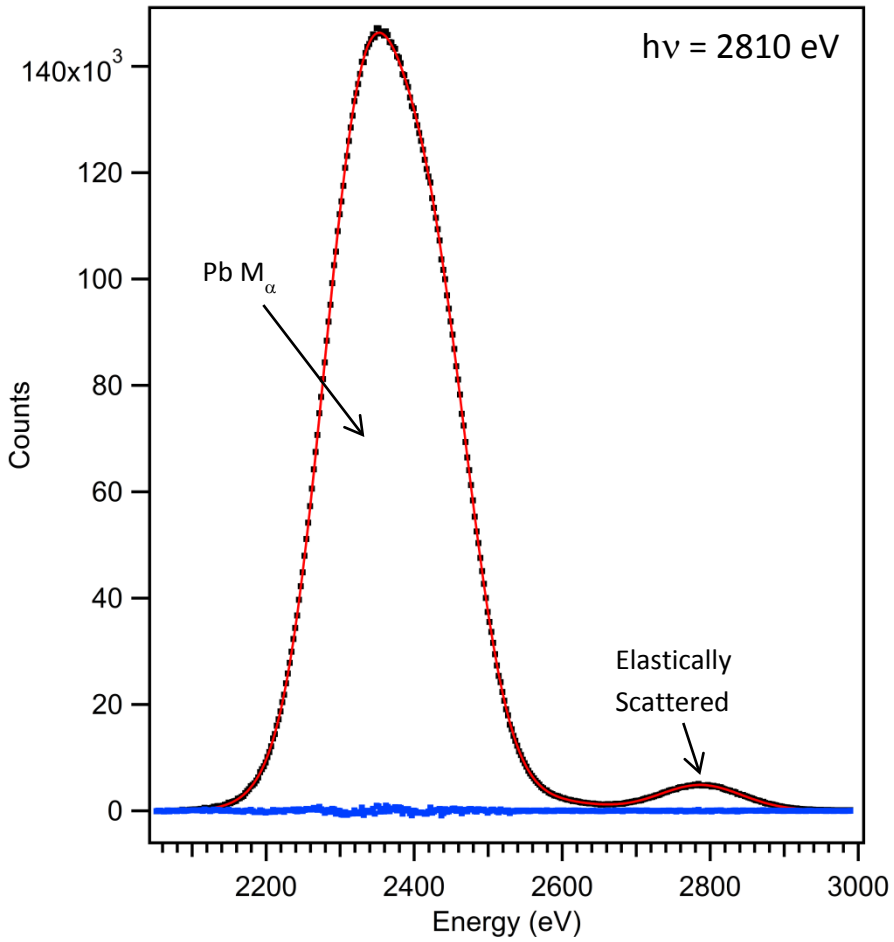

Figure S. I. 5: XRF spectrum of $PbCl_2$ taken with a photon energy of 2810 eV (black dots). The red curve is a fit to the spectrum and the blue dots are the difference between the collected data (black dots) and the fitted spectrum (red curve). The standard deviation of the blue dots is used as a measure of the standard deviation of the data. (See text for details.)

Figure S. I. 6

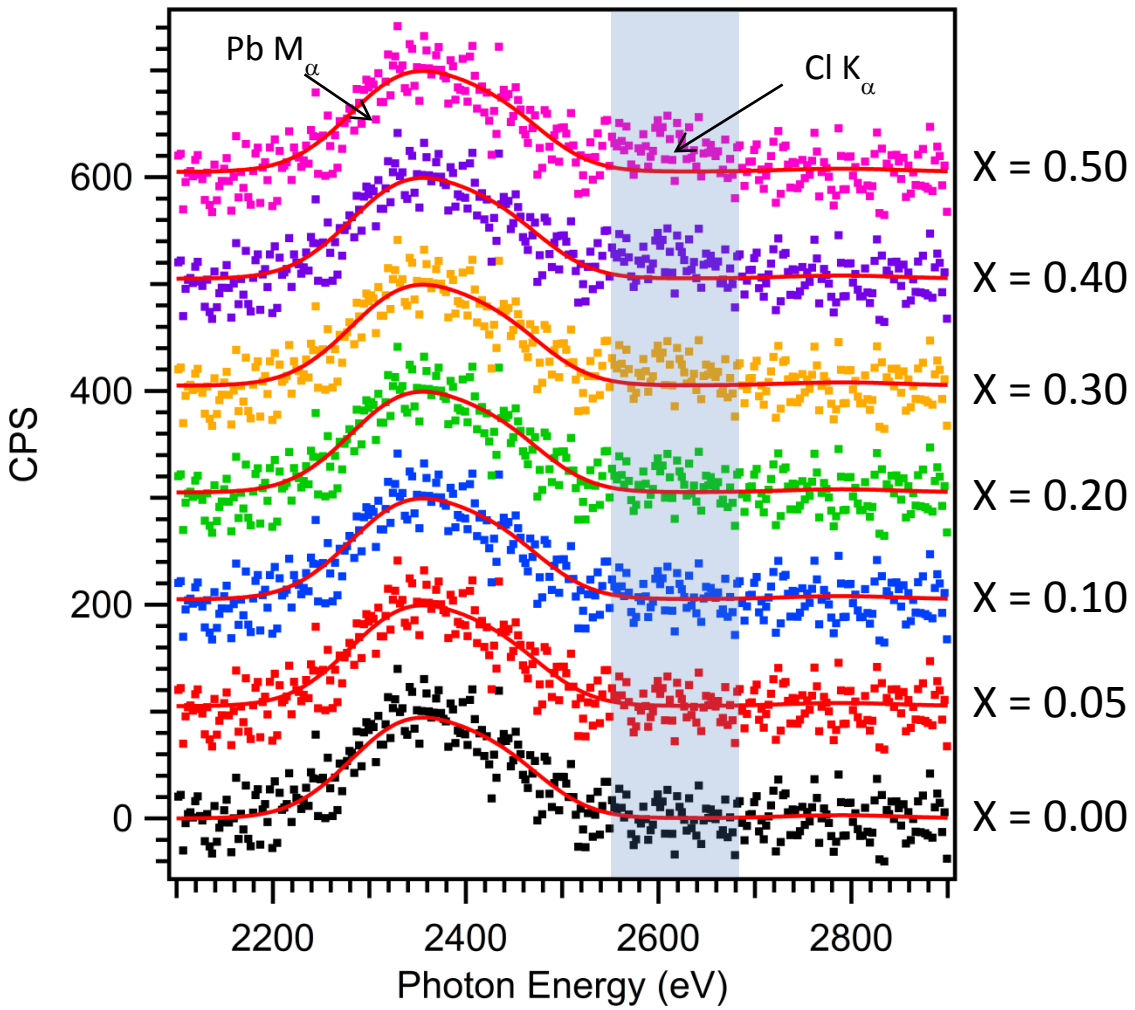

Figure S. I. 6: XRF spectra representative of those used to collect the FY-XAS spectrum shown in Figure 3, blue. The black dots are calculated by scaling the fitted spectrum in Figure S. I. 5 (red line) and adding noise representative of the XRF spectra used for the FY-XAS spectra (see text for details). The red, blue, green, orange, purple, and pink spectra include contributions that would be expected for Cl concentrations in the perovskite of x = 0.05, x = 0.10, x = 0.20, x = 0.30, x = 0.40, and x = 0.50 respectively. The energy window integrated for the FY-XAS spectra is indicated by the light blue box.

References

[1] Werner, W. S. M.; Smekal, W.; Powell, C. J. *NIST Database for the Simulation of Electron Spectra for Surface Analysis, Version 1.3*, National Institute of Standards and Technology: Gaithersburg, MD, USA, 2011.

[2] Baikie, T.; Fang, Y.; Kadro, J. M.; Schreyer, M.; Wie, F.; Mhaisalkar, S. G.; Graetzel, M.; White, T. J.; Synthesis and Crystal Chemistry of the Hybrid Perovskite $(CH_3NH_3)PbI_3$ for Solid-State Sensitized Solar Cell Applications. *J. Mater. Chem. A*, **2013**, *1*, 5628 – 5641.

[3] Kim, H. S.; Lee, C. R.; Im, J. H.; Lee, K. -B.; Moehl, T.; Marchioro, A.; Moon, S. J.; Humphry-Baker, R.; Yum, J. H.; Moser, J. E.; Grätzel, M.; Park, N. G. Lead Iodide Perovskite Sensititzed All-Solid-State Submicron Thin Film Mesoscopic Solar Cell with Efficiency Exceeding 9%. *Sci. Rep.* **2012**, *2*, 591 – 597.

[4] *CRC Handbook of Chemistry and Physics, 45th ed.*; The Chemical Rubber Company: Cleveland, OH, 1964.

[5] Welte, A.; Waldauf, Ch.; Brabec, Ch.; Wellmann, P. J. Application of Optical Absorbance for the Investigation of Electronic and Structural Properties of Sol-Gel Processed TiO_2 Films. *Thin Sol. Films* **2008**, *516*, 7256 – 7259.

[6] Himpsel, F. J.; McFeely, F. R.; Taleb-Ibrahimi, A.; Yarmoff, J. A.; Hollinger, G. Microscopic Structure of the SiO_2/Si Interface. *Phys. Rev. B* **1988**, *38*, 6084 – 6096.

[7] Trzhaskovskaya, M. B.; Nikulin, V. K.; Nefedov, V. I.; Yarzhemsky, V. G. Non-dipole second order parameters of the photoelectron angular distribution for elements Z = 1 – 100 in the photoelectron energy range 1 – 10 keV *Atomic Data and Nuclear Data Tables* **2006**, *92*, 245 – 304.

[8] Trzhaskovskaya, M. B.; Nefedov, V. I.; Yarzhemsky, V. G. Photoelectron angular distribution parameters for elements Z = 55 to Z = 100 in the photoelectron energy range 100 – 5000 eV. *Atomic Data and Nuclear Data Tables* **2002**, *82*, 257 – 311.

[9] Henke, B. L.; Gullikson, E. M.; Davis, J. C. X-ray Interactions: Photoabsorption, Scattering, Transmission, and Reflection at E = 50 – 30000 eV, Z = 1 – 92. *Atomic Data and Nuclear Data Tables* **1993**, *54*, 181 – 342.

[10] Baikie, T.; Fang, Y.; Kadro, J. M.; Schreyer, M.; Wie, F.; Mhaisalkar, S. G.; Graetzel, M.; White, T. J. Synthesis and Crystal Chemistry of the Hybrid Perovskite $(CH_3NH_3)PbI_3$ for Solid-State Sensitised Solar Cell Applications. *J. Mater. Chem. A* **2013**, *1*, 5628 – 5641.